ATP Hydrolysis in the β_{TP} and β_{DP} Catalytic Sites of F_1-ATPase

Markus Dittrich,*† Shigehiko Hayashi,‡§ and Klaus Schulten*†

*Beckman Institute, University of Illinois at Urbana-Champaign, Urbana, Illinois 61801; †Department of Physics, University of Illinois at Urbana-Champaign, Urbana, Illinois 61801; ‡Theoretical Chemistry Division, Fukui Institute for Fundamental Chemistry, Kyoto University, Kyoto 606-8103, Japan; and §Japan Science and Technology Agency, Kawaguchi, Saitama, Japan

ABSTRACT The enzyme F_1-adenosine triphosphatase (ATPase) is a molecular motor that converts the chemical energy stored in the molecule adenosine triphosphate (ATP) into mechanical rotation of its γ-subunit. During steady-state catalysis, the three catalytic sites of F_1 operate in a cooperative fashion such that at every instant each site is in a different conformation corresponding to a different stage along the catalytic cycle. Notwithstanding a large amount of biochemical and, recently, structural data, we still lack an understanding of how ATP hydrolysis in F_1 is coupled to mechanical motion and how the catalytic sites achieve cooperativity during rotatory catalysis. In this publication, we report combined quantum mechanical/molecular mechanical simulations of ATP hydrolysis in the β_{TP} and β_{DP} catalytic sites of F_1-ATPase. Our simulations reveal a dramatic change in the reaction energetics from strongly endothermic in β_{TP} to approximately equienergetic in β_{DP}. The simulations identify the responsible protein residues, the arginine finger αR373 being the most important one. Similar to our earlier study of β_{TP}, we find a multicenter proton relay mechanism to be the energetically most favorable hydrolysis pathway. The results elucidate how cooperativity between catalytic sites might be achieved by this remarkable molecular motor.

INTRODUCTION

More than three decades of intensive research have uncovered a wealth of information about F_1F_o-adenosine triphosphate (ATP) synthase, the enzyme responsible for the synthesis of ATP, the cell's energy currency (Boyer, 1993, 1997; Cross, 2000; Senior et al., 2002). Groundbreaking imaging experiments on isolated F_1 units by Noji et al. (1997) proved that the enzyme operates as an ATP powered rotatory molecular motor. This provided further support for the conjecture that F_1F_o-ATP synthase operates as two coupled molecular motors: F_o being driven by a transmembrane proton gradient generated during photosynthesis or oxidative phosphorylation (Junge et al., 1997; Rastogi and Girvin, 1999; Fillingame et al., 2002; Angevine and Fillingame, 2003; Aksimentiev et al., 2004) and, via coupling to F_1 by a central stalk, powering the rotatory conformational changes in F_1 that eventually lead to the synthesis of ATP.

The protein complex can be separated into its two constituent structural units. This gave rise to a vast amount of biochemical data on the soluble F_1 part and eventually led to the determination of the first x-ray structure of F_1 in 1994 by Abrahams et al. (1994). However, despite this wealth of information, we still lack a thorough understanding of how the catalytic sites achieve efficient catalysis and are able to couple in a highly cooperative fashion a chemical event to mechanical rotation of the stalk. This study seeks to address those questions and provides insight into how this is achieved by F_1.

Individual F_1 units retain the ability to hydrolyze ATP (Boyer, 1993; Senior et al., 2002) and can convert the free energy thereby released into mechanical work (Noji et al., 1997; Yasuda et al., 2001). In its simplest prokaryotic form, F_1 consists of five distinct subunits in the stoichiometry $(\alpha\beta)_3\gamma\delta\epsilon$. The hexamerically arranged $(\alpha\beta)_3$ part contains the three catalytic binding sites at the interface between adjacent α- and β-subunits and undergoes cyclic conformational changes upon ATP hydrolysis, thereby driving the rotation of the γ-stalk.

Biochemical data revealed that during steady-state hydrolysis the three catalytic binding pockets in F_1 do not operate individually but rather in a cooperative fashion. At any given moment during the rotatory catalytic cycle, each binding pocket is in a different conformation corresponding to a particular stage along the ATP hydrolysis pathway. This is evidenced by the fact that during steady-state hydrolysis the three binding pockets exhibit different binding affinities for ATP, i.e., there is a high, a medium, and a low affinity site with K_d values for ATP of $\leq$50 nmol, 0.5 μmol, and 25 μmol, respectively (Weber et al., 1994). This and additional biochemical evidence led to the proposal of a binding change mechanism by Boyer (1993) to be characteristic for F_1-ATPase's modus operandi. This correlated well with imaging experiments (Noji et al., 1997) showing the rotation of the central stalk in steps of 120° that were later resolved into a 90° and a 30° substep (Yasuda et al., 2001; Shimabukuro et al., 2003; Nishizaka et al., 2004).

The determination of several high resolution x-ray structures (Abrahams et al., 1994; Gibbons et al., 2000; Menz et al., 2001) has provided atomic level details of F_1-ATPase as a whole and its catalytic sites in particular. For the first time, it was possible to correlate the findings of

Submitted May 17, 2004, and accepted for publication August 2, 2004.

Address reprint requests to Klaus Schulten, Beckman Institute, University of Illinois at Urbana-Champaign, 405 N. Mathews Ave., Urbana, IL 61801. Tel.: 217-244-1604; Fax: 217-244-6078; E-mail: kschulte@ks.uiuc.edu

0006-3495/04/11/2954/14 $2.00

doi: 10.1529/biophysj.104.046128

biochemical mutation studies with the conformation of the respective protein residues in the structural context of the complete enzyme. For the catalytic sites this meant that the effect of specific protein side chains on the hydrolysis reaction could be related to their spatial location with respect to the nucleotide. This permitted the identification of several residues important for, e.g., nucleotide binding or catalytic transition state stabilization (Ren and Allison, 2000; Senior et al., 2002).

The analysis of biochemical data in terms of the available x-ray structures as well as the interpretation of the structures themselves, however, is complicated by the fact that the x-ray data provides an inherently static picture from which the causal chain of events during rotatory catalysis cannot be inferred directly. This is further complicated by the fact that it is not clear which of the three catalytic sites captured in the crystal structures correspond to the high, medium, and low affinity binding pockets observed in experiment. As for the hydrolysis reaction itself, a thorough understanding of the transition state structure is clearly desirable. Unfortunately, it is not obvious that the available structures crystallized in the presence of so-called transition state analogs do provide a faithful representation of the transition state. From a functional point of view, we still lack an understanding of how ATP hydrolysis is coupled to larger scale conformational motions eventually leading to the rotation of the central stalk and of how the cooperation between catalytic sites during steady-state catalysis is effected.

This is where computational modeling can advance our understanding of F_1 on a microscopic as well as on a higher functional level. Computer simulations allow one to probe the dynamics of stalk rotation and its effect on the catalytic sites (Böckmann and Grubmüller, 2002), the energetics of the hydrolysis reaction in the binding pockets (Dittrich et al., 2003; Gao et al., 2003; Strajbl et al., 2003; Yang et al., 2003), and the coupling mechanism between individual binding sites. Several computer simulations investigating nucleotide hydrolysis reactions and nucleotide binding in systems other than F_1 have been published (Glennon et al., 2000; Langen et al., 1992; Schweins et al., 1994; Cavalli and Carloni, 2001; Okimoto et al., 2001; Minehard et al., 2002; Li and Cui, 2004) and have contributed to a better understanding of the underlying microscopic events. Warshel and co-workers (Strajbl et al., 2003) have recently used the semimicroscopic version of the protein dipole Langevin dipoles/linear response approximation (PDLD/S-LRA) and empirical valence bond (EVB) method to examine the energetics of F_1-ATPase and found that electrostatic effects play a dominating role in efficient catalysis. In a previous publication, we used an ab initio quantum mechanical/molecular mechanical (QM/MM) methodology to thoroughly analyze the energetics of ATP hydrolysis in the β_{TP} binding pocket of F_1-ATPase (Dittrich et al., 2003). We were able to show that efficient ATP hydrolysis in β_{TP} proceeds along a multicenter proton pathway and that the catalytic site in the conformation studied stabilizes the reactant ATP rather than promoting the catalytic reaction. β_{TP} was therefore identified with the high affinity site, which tightly binds ATP but not yet induces its chemical transformation.

In this study, we have used a combined QM/MM methodology (Warshel, 1976; Singh and Kollman, 1986; Field et al., 1990; Lyne et al., 1999; Hayashi et al., 2001; Dittrich et al., 2003) to study the ATP hydrolysis reaction in F_1-ATPase. QM/MM simulations allow one to use quantum mechanical methods to simulate chemical events inside an extended protein environment that is being modeled classically. Such a treatment is mandatory for a proper description of enzymatic reactions, which are influenced to a large degree by the electrostatic environment of the surrounding protein (Warshel, 1991, 2003; Strajbl et al., 2003). Using QM/MM simulations, we have extended our previous simulations of β_{TP} to the β_{TP} and β_{DP} catalytic sites of F_1-ATPase at a much improved QM description, and we have analyzed both in terms of their efficacy for ATP hydrolysis, their cooperative capabilities, and their ability to couple the chemical reaction to larger scale mechanical motions of the γ-stalk.

METHODS

β_{TP} catalytic site

The system setup used in our QM/MM simulations of β_{TP} is identical to the one described in Dittrich et al. (2003), and the reader is therefore referred to this publication for further details. The quantum mechanically treated region comprises the triphosphate backbone of ATP (ATPa), the side chains of βK162, βE188, and βR189 as well as five water molecules WAT1–WAT5 surrounding the γ-phosphate as shown in Fig. 1 *a*. Our QM/MM code is based on the quantum chemistry package GAMESS (Schmidt et al., 1993) and uses the AMBER force field (Cornell et al., 1995) to describe the interactions in the region treated by molecular mechanics. In contrast to our previous simulations, the calculations in this study included electron correlation effects and treated the QM core region using density functional theory (DFT) at the B3LYP/6-31G level of theory. To render these computationally expensive QM/MM calculations feasible, the simulations were performed on 8–32 EV7 processors (1.15Ghz) at the Pittsburgh Supercomputing Center.

β_{DP} catalytic site

The preparation of the QM/MM subsystem for β_{DP} proceeded analogously to β_{TP} and it was extracted from the same equilibrated full F_1 structure. To minimize the total charge, the subsystem included all residues closer than 19.8 Å (instead of 20 Å for β_{TP}) to the nucleotide. The ADP present in β_{DP} of the original structure (pdb access code 1E79) was replaced by ATP, and the subsystem was then subjected to 500 ps of molecular dynamics (MD) equilibration followed by 100 ps of simulated annealing and further minimization until a root mean-square (RMS) gradient $\leq 10^{-5}$ Hartree/Bohr was reached. The resulting conformation constituted the starting structure for the QM/MM simulations.

The quantum mechanically treated core region in β_{DP} contained all the groups present in β_{TP} as described above. The partitioning of the subsystem into the QM and MM segments was carried out as specified in our previous study for β_{TP} (Dittrich et al., 2003). In addition, the QM region in β_{DP} included the guanidinium group of αR373 that is situated close to the β- and

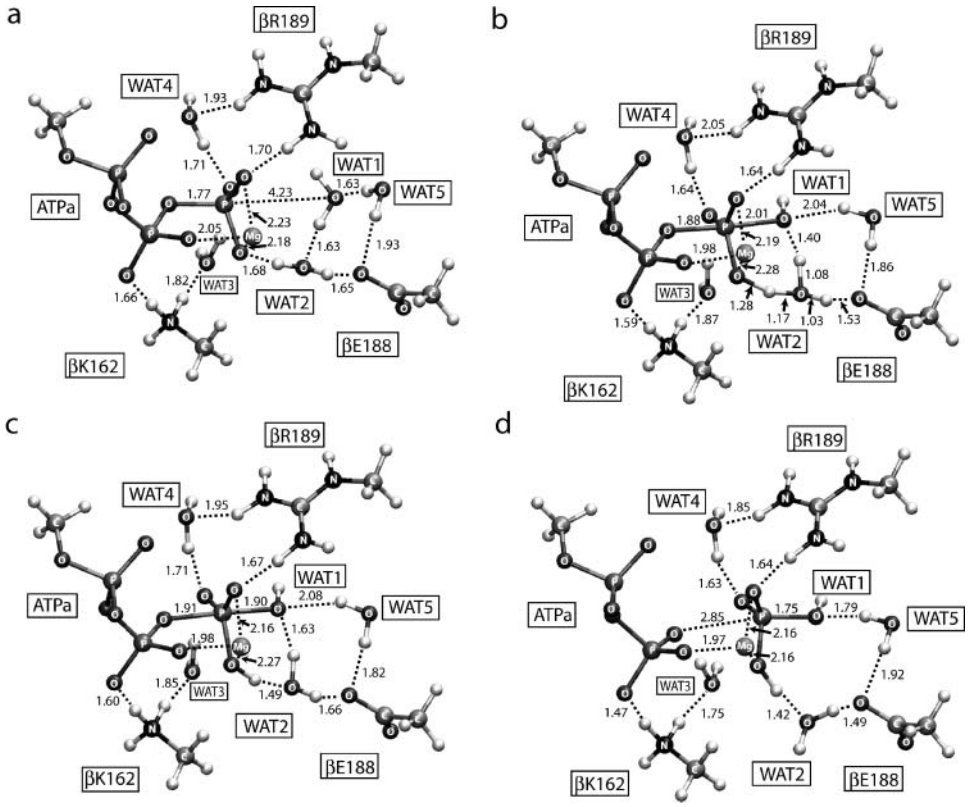

FIGURE 1 Conformational snapshots of the β_{TP} catalytic site along the ATP hydrolysis pathway. Shown is the structure of the QM segment in the reactant (*a*), transition (*b*), intermediate (*c*), and final (*d*) state together with important bond lengths. All nonhydrogen atoms are labeled according to their atom type.

γ-phosphate groups of ATP (cf. Fig. 3 *a*). Similarly to βR189, the side chain of αR373 was separated into QM and MM segments at the C_γ–C_δ bond. As before, the link atom approach was used to cap the free valences at the frontier bonds between the QM and the MM regions. All QM/MM calculations were performed at the B3LYP/6-31G level of theory. Saddle points were validated by the presence of a single imaginary frequency in the Hessian matrix, and intrinsic reaction coordinate calculations were used to connect the transition state with the intermediate and prehydrolysis states (cf. Results).

We also performed the two mutations αR373G and βR260C in β_{DP} and studied the resulting binding sites computationally. The program DOWSER (Zhang and Hermans, 1996) was used to examine if the resulting cavities should be filled with additional water molecules. In the case of αR373G, DOWSER suggested the placement of a single water molecule hydrogen bonded to the β- and γ-phosphate groups. Optimization of this conformation, however, led to an unnatural ligation of the magnesium ion, and this water molecule was therefore rejected. This instability is likely related to the finding that in β_{TP} and hence without the presence of αR373's guanidinium group next to the phosphate backbone there is a change in the ligation pattern of Mg^{2+} (cf. Results). Such a structural change cannot be captured via optimization, and, as observed, the addition of a water molecule close to the phosphate backbone and the magnesium ion leads to an unstable conformation. For βR260C, DOWSER suggested the placement of three water molecules that turned out to be stable under optimization and that were therefore accepted. For both mutations, we reoptimized the reactant and final state geometries, using the conformations of the wild-type system as starting points. The determination of the respective transition state conformations was not carried out. The size of the QM/MM system renders this computationally very demanding and typically requires a large number of constrained optimizations and Hessian matrix calculations that were beyond our computational capabilities. It should be pointed out that these mutation studies cannot be unequivocally related to experimental results. This is due to the possibility that in experiments mutations might lead to larger scale structural rearrangements that are not sampled in our optimizations. In contrast to experiments, our mutation studies provide a rather direct probe of the immediate effect of particular residues on the chemical reaction.

In both β_{TP} and β_{DP}, all R, K, E, and D residues close to the nucleotide were chosen to be in their ionized states similar to the choice of Strajbl et al. (2003). To estimate the Coulomb interaction between the catalytically active region and the remainder of the protein environment, we calculated the atomic restrained electrostatic potential (RESP) charges (Baily et al., 1993) on a reduced QM system consisting of only ATPa and the five water molecules WAT1–WAT5. The Coulomb interactions between the reduced QM and the MM region at the optimized reactant and transition state conformations of the full QM/MM system were then calculated classically. This approximation correctly represents the relative magnitude of interactions, even though the absolute values are likely not accurate.

All the energies provided in this article refer to reaction enthalphies rather than true free energies, since the latter are beyond our computational capabilities. However, as done in Dittrich et al. (2003), one can argue convincingly that the calculated reaction enthalpies properly characterize ATP hydrolysis and the relative energies of reaction intermediates inside the catalytic binding pockets.

RESULTS

The following section describes the results of our study of ATP hydrolysis in the β_{TP} and β_{DP} catalytic sites of F_1 using QM/MM simulations. The computational system for β_{TP} is identical to the one employed in our previous study (Dittrich et al., 2003); the use of a more sophisticated QM description, however, necessitates a thorough reexamination of its properties to allow for a meaningful comparison with β_{DP}.

The system setup for the β_{DP} catalytic site proceeded in an analogous fashion and is described in Methods. The makeup of the QM core region in β_{DP} was chosen to be similar to the one for β_{TP}, the main difference being the presence of the guanidinium side chain of αR373 that is now oriented toward the β- and γ-phosphate groups of ATP. In β_{TP}, this residue is found to be oriented away from the phosphate group (Gibbons et al., 2000; Dittrich et al., 2003) and, therefore, was not included in the QM description.

To elucidate the mechanism of ATP hydrolysis in F_1, it is necessary to examine and compare the catalytic properties of its binding sites in different conformations along the rotatory catalytic cycle. This investigation of β_{TP} and β_{DP} constitutes a step toward this goal. We first summarize our results for ATP hydrolysis in β_{TP} that include electron correlation effects not captured in our previous study. We then give a detailed description of the simulation results for β_{DP} and relate them to the findings for β_{TP}.

Study of ATP hydrolysis reaction in the β_{TP} catalytic site

Reactant state

The conformation of the reactant state is depicted in Fig. 1 *a*. Compared to our previous findings reported in Dittrich et al. (2003), the inclusion of electron correlation leads to an elongation of the phosphoester bonds and a tightening of the arrangement of water molecules around the γ-phosphate but to only minor structural changes for the rest of the system.

Table 1 lists the Mulliken charges for the reactant, transition, intermediate, and final states obtained in this study. A comparison of the Mulliken charges in the reactant state with the corresponding values obtained in our previous study reveals a significant increase in charge transfer between the phosphate backbone and the side chains of βK162, βE188, and βR189 as well as Mg^{2+}. The change in charge transfer between different states along the reaction path, however, is of similar magnitude in this and the past study supporting the validity of our previous Hartree-Fock description.

Transition state

The conformation of the transition state in β_{TP} was determined as described in Methods and is depicted in Fig. 1 *b*. The transition state features a planar pentacovalent arrangement of the γ-phosphate group and evolves via a multicenter proton relay mechanism giving rise to a hydronium ion-like arrangement located between ATP-P_γ and βE188 consisting of WAT2 and a proton derived from WAT1.

The data in Table 1 shows that the Mulliken charge on the hydronium ion in the transition state is reduced by 0.26 e compared to the value obtained in our previous study. Its smaller magnitude allows for a more efficient charge stabilization in the transition state by the protein environment, thereby contributing to a reduction in the transition state barrier of the hydrolysis reaction.

Intermediate and final state

After passing the transition state, the system exhibits bond formation between the nucleophilic oxygen and P_γ in

TABLE 1 Mulliken charges on important groups for the reactant, transition, intermediate, and product conformation of β_{TP} and β_{DP} derived from B3LYP/6-31G

	Reactant state		Transition state		Intermediate state		Final state	
Group name	β_{TP}	β_{DP}	β_{TP}	β_{DP}	β_{TP}	β_{DP}	β_{TP}	β_{DP}
ATP*	−3.17	−3.20	−3.29	−3.26	−3.25	−3.19	−3.36	−3.27
ADP†	−2.13	−2.18	−2.28	−2.28	−2.30	−2.28	−2.44	−2.34
P_i‡	−1.02	−1.04	−0.94	−0.96	−0.89	−0.92	−0.76	−0.93
Mg^{2+}	1.52	1.65	1.50	1.63	1.50	1.63	1.49	1.61
WAT1	0.00	−0.03	–	–	–	–	–	–
WAT2§	−0.07	−0.09	0.02	0.05	−0.03	0.02	−0.02	0.01
H_3O^+¶	–	–	0.45	0.48	–	–	–	
WAT3	0.00	−0.03	−0.02	−0.03	0.00	−0.04	0.00	−0.01
WAT4	0.00	−0.10	−0.03	−0.10	−0.02	−0.10	0.00	−0.08
WAT5	−0.10	−0.05	−0.10	−0.04	−0.10	−0.04	−0.09	−0.03
βE188	−0.78	−0.71	−0.75	−0.71	−0.77	−0.74	−0.75	−0.72
βR189	0.81	0.88	0.87	0.87	0.86	0.86	0.84	0.87
βK162	0.80	0.84	0.78	0.81	0.78	0.82	0.73	0.80
αR373	–	0.85	–	0.81	–	0.81	–	0.81

*ATP refers to the collection of atoms belonging to ATP in the reactant state.

†ADP refers to the collection of atoms belonging to ADP in the reactant state.

‡P_i refers to the collection of atoms including P_γ,$O_{\gamma1}$, $O_{\gamma2}$, $O_{\gamma3}$ of ATP, WAT1–O, WAT1–H_1, and WAT2–H_1.

§WAT2 in the reactant and transition state consists of the collection of atoms belonging to WAT2 in the reactant state. After the proton transfer, WAT2 in the intermediate and the final state consists of WAT1–H_2, WAT2–O, and WAT2–H_2.

¶H_3O^+ consists of WAT1–H_2, WAT2–H_1, WAT2–O, and WAT2–H_2.

the intermediate state shown in Fig. 1 *c*. This state has an S_N2-like conformation with almost identical bond lengths between P_γ and the attacking and leaving groups. The γ-phosphate group is approximately planar and has a pentacovalent arrangement of its ligands. Furthermore, proton transfer between the hydronium ion present in the transition state and ATP-$O_{\gamma 1}$ takes place, thereby completing the transfer initiated by the nucleophilic water.

The final state conformation evolves from the intermediate structure by further separation of ADP and P_i along the $O_{\beta 3}$–P_γ bond. The main effect of electron correlation in the final state is a decrease in distance between products ADP and P_i from 3.00 Å to 2.85 Å.

Energetics of ATP hydrolysis and interactions in β_{TP}

The relatively minor changes in conformation between this and the previous study (Dittrich et al., 2003) manifest themselves in similar potential energy profiles along the reaction path. Fig. 4 *a* depicts the energetics in β_{TP} and, as in our previous study, we find that ATP hydrolysis in β_{TP} is endothermic and, thereby, favors ATP synthesis over its hydrolysis. The final state energy lies ~19 kcal/mol above the value in the reactant state, and the overall energy profile is relatively flat after passage of the transition state. Previously, we determined the state energies using single-point MP2//HF/6-31G calculations. Full geometry reoptimization via DFT leads to further lowering of the energies of all states and yields a transition state barrier of 25.5 kcal/mol (cf. Fig. 4 *a*).

A multicenter proton relay mechanism is found to be energetically favorable compared to direct proton transfer, the latter mechanism exhibiting a transition state barrier of 48.1 kcal/mol at the B3LYP/6-31G level of theory (data not shown).

When considering the changes in Coulomb interaction between reactant and transition state (cf. Fig. 5) one, too, observes qualitative agreement with our previous study (data not shown). The three main contributions to the change in Coulomb interaction are due to the side chains of βK162, βE188, and βR189, and their interpretation in the context of the previously proposed reaction mechanism is similar. As a corollary it follows that the MP2//HF/6-31G level of theory employed in our previous study does provide a qualitatively correct picture of the ATP hydrolysis reaction in F_1.

In summary, our DFT QM/MM study of ATP hydrolysis in β_{TP} shows that the chemical reaction proceeds via a multicenter proton relay mechanism and is endothermic. The β_{TP} catalytic site, therefore, binds ATP tightly and does promote ATP synthesis rather than its hydrolysis.

Study of ATP hydrolysis reaction in the β_{DP} catalytic site

Reactant state

The major difference in the quantum mechanically treated core region of β_{DP} compared to β_{TP} is the presence of the guanidinium group of αR373 that is hydrogen bonded to ATP-$O_{\alpha 2}$, ATP-$O_{\beta 3}$, and ATP-$O_{\gamma 3}$. This is shown in Fig. 2 that gives a schematic representation of the hydrogen bonding network in the catalytic sites and clearly reveals the increased number of interactions between the nucleotide and the binding pocket present in β_{DP} compared to β_{TP}. The side chain of αR373 plays the role of the well-known arginine finger provided by the guanosine triphosphatase (GTPase)-activating protein during guanosine triphosphate hydrolysis in, e.g., Ras (Wittinghofer et al., 1997).

Fig. 3 *a* shows the reactant state conformation of the QM segment in β_{DP}. The guanidinium group of βR189 is located next to the one of αR373 and forms strong hydrogen bonds with two γ-phosphate oxygens. This is different from the situation in β_{TP} where only one of the guanidinium hydrogens of βR189 is bonded to ATP-$O_{\gamma 2}$, the other one being coordinated to a water molecule, WAT4 (cf. Fig. 1 *a*). This change in bonding pattern of βR189 is due to a reorientation of the γ-phosphate group as a whole compared to β_{TP}. An important ramification of this motion is a change in the ligation pattern as well as in the bonding distances of the magnesium ion. In β_{DP}, Mg^{2+} interacts with only ATP-$O_{\beta 2}$ and ATP-$O_{\gamma 2}$ while being ligated to ATP-$O_{\beta 2}$, ATP-$O_{\gamma 1}$, and

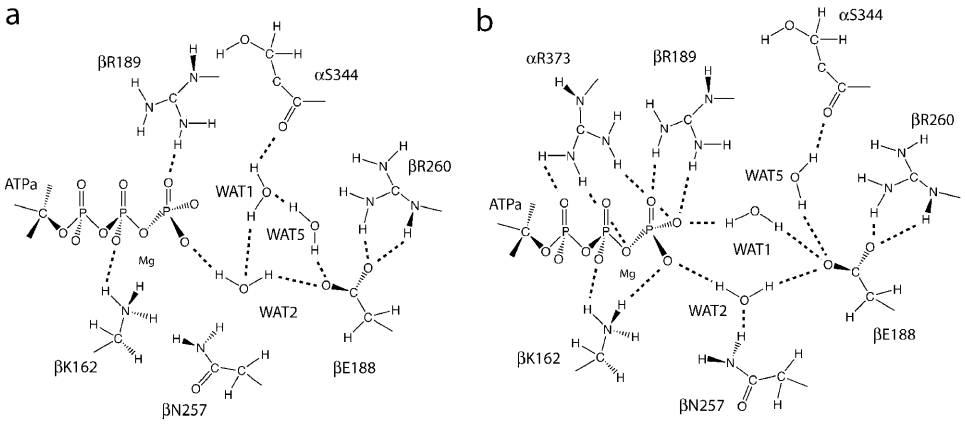

FIGURE 2 Comparison of hydrogen bonding network in β_{TP} and β_{DP}. The short dashed lines indicate hydrogen bonds between important protein residues, water molecules, and the phosphate backbone of ATP in β_{TP} (*a*) and β_{DP} (*b*).

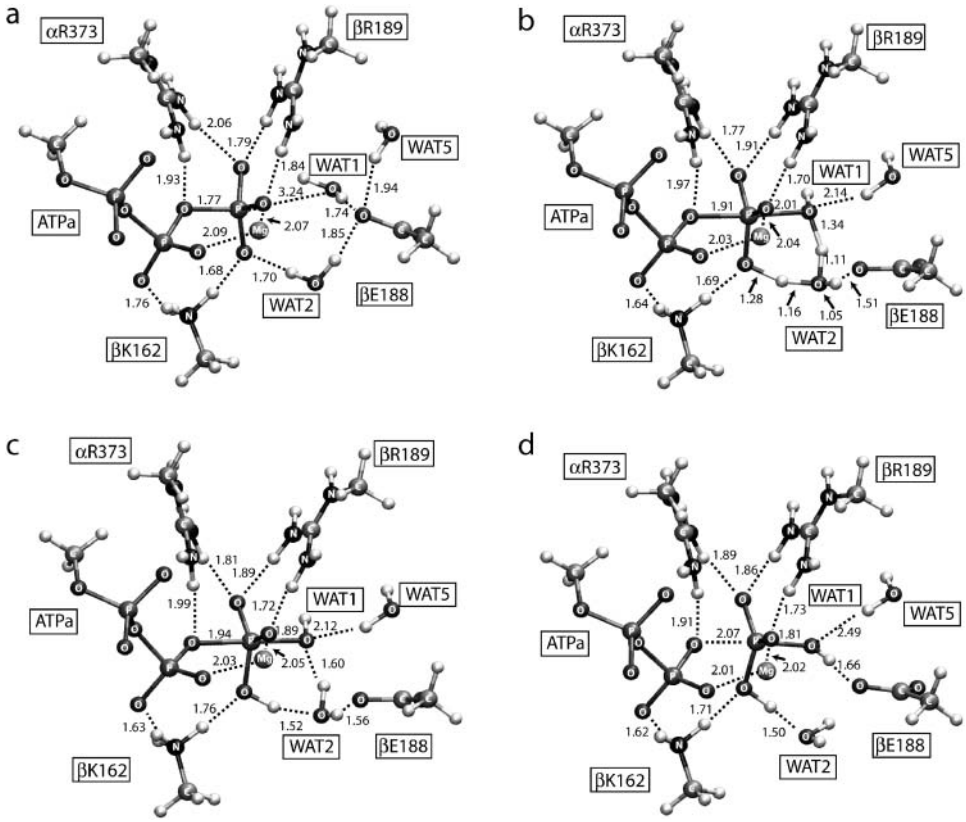

FIGURE 3 Conformational snapshots of the β_{DP} catalytic site along the ATP hydrolysis pathway. Shown is the structure of the QM segment in the reactant (*a*), transition (*b*), intermediate (*c*), and final (*d*) state together with important bond lengths. All nonhydrogen atoms are labeled according to their atom type. Water molecules WAT3 and WAT4 are not shown for clarity.

ATP-$O_{\gamma 2}$ in β_{TP}. The bond thus liberated is accepted by a water molecule. Interestingly and in contrast to the situation in β_{TP}, the reorientation of the γ-phosphate group causes the coordination of Mg^{2+} in β_{DP} to be almost ideally octahedral and therefore seems to be primed for efficient catalysis (Bernal-Uruchurtu and Ortega-Blake, 1995).

In contrast to β_{TP}, WAT5, the water molecule hydrogen bonded to αS344, is not in a good position to initiate nucleophilic attack since it recedes by more than 1 Å from P_γ compared to β_{TP}. This is due to an increase in the αS344-O–P_γ distance from 4.46 Å to 5.84 Å in going from β_{TP} to β_{DP} in addition to a slight rotation of the α-helix containing αS344. The role of the nucleophilic water in β_{DP} is played by a water molecule hydrogen bonded to ATP-$O_{\gamma 3}$ and βE188-$O_{\epsilon 1}$ whose oxygen atom is located only 3.24 Å away from P_γ. To be consistent with the numbering scheme in β_{TP}, this water molecule will be called WAT1. Even though αS344 does not coordinate the nucleophilic water directly, the tight hydrogen bonding network present between water molecules in the nucleophilic region and this residue makes the latter a potentially important factor in initiating nucleophilic attack as proposed in Dittrich et al. (2003). The water molecule WAT2 forms a strong hydrogen bond with the amide hydrogen of βN257 (cf. Fig. 2); in β_{TP}, this residue is more than 4 Å away from WAT2. The ammonium group of βK162 is hydrogen bonded to two phosphate oxygens, ATP-$O_{\beta 1}$ and ATP-$O_{\gamma 1}$, due to the aforementioned reorientation of the γ-phosphate group. The latter replaces the hydrogen bond to WAT3 found in β_{TP}.

The side-chain conformation of βE188, particularly in regard to the nucleotide, changes markedly between β_{TP} and β_{DP}. With respect to the ATP-$O_{\beta 3}$–P_γ–$O_{\gamma 2}$ plane in β_{DP}, βE188-$O_{\epsilon 1}$ is almost in plane, whereas in β_{TP} the whole side chain is located significantly out of plane. Hence, even though the conformations of β_{TP} and β_{DP} considered in this study look similar overall, there are small but significant differences in the precise location of important protein side chains close to the catalytic site.

Interestingly, evaluation of the intrinsic reaction coordinates from the transition state toward the reactant state showed that the system exhibits an intermediate prehydrolysis state, which is energetically slightly above the reactant state. Structurally and compared to the reactant conformation, this state is characterized by a change in the hydrogen bonding network surrounding the nucleophilic WAT1. Incidentally, its conformation is very similar to the reactant state in β_{TP}, the major difference being that the nucleophilic water is hydrogen bonded to ATP-$O_{\gamma 3}$ instead of αS344. In the prehydrolysis state conformation, WAT1 is hydrogen bonded to WAT2 and ATP-$O_{\gamma 3}$, WAT3 hydrogen bonds to βE188 and WAT2, and WAT5 hydrogen bonds to WAT1 and αS344. The formation of a hydrogen bond between WAT1 and WAT2 is accompanied by a movement of WAT2 toward WAT1 by ~0.6 Å and causes the hydrogen bond

between WAT2-O and βN257 to break. Furthermore, a water molecule in the MM segment coordinating Mg^{2+} switches its hydrogen bond from WAT2 to βE188. The hydrogen bonding pattern established in this prehydrolysis state persists over the full course of the hydrolysis reaction. It is, therefore, used as a reference state to compute the change in Coulomb interactions between reactant and transition state (cf. Fig. 5) to avoid spurious peaks caused by the rearrangement of the hydrogen bonding network.

The Mulliken charges for the reactant state in β_{DP} are similar to the ones calculated in β_{TP} with the exception of Mg^{2+}, which increases its charge by 0.13 e. This can be attributed to the difference in bonding pattern between the magnesium ion and the phosphate backbone of ATP.

Transition state

The transition state in β_{DP} evolves from the reactant and prehydrolysis state upon nucleophilic attack of WAT1 and is depicted in Fig. 3 *b*. Of particular importance is the fact that, similar to the situation in β_{TP}, our simulations show that ATP hydrolysis proceeds via a multicenter proton relay mechanism rather than direct proton transfer from the nucleophilic water to the γ-phosphate group. The transition state barrier for direct proton transfer in β_{DP} is 31.6 kcal/mol (data not shown) and therefore significantly higher. The proton of the nucleophilic water is first transferred to WAT2 that then donates its proton to the γ-oxygen to complete the proton transfer. This leads to a hydronium ion in the transition state that is formed by WAT1's proton, WAT2; the hydronium ion is located between the γ-phosphate group and the carboxyl side chain of βE188. The conformation of the pentacovalent phosphate group in the transition state is qualitatively similar to the one in β_{TP}, the main difference being the presence of the guanidinium group of αR373 and the changes in bonding pattern of Mg^{2+} with the phosphate backbone and water molecules.

Compared to β_{TP}, the distances between WAT1's transferred proton and WAT1-O/WAT2-O are slightly decreased/increased, respectively, giving rise to a somewhat earlier transition state. In the transition state the guanidinium group of αR373 binds significantly stronger to the γ-phosphate compared to the reactant state. The hydrogen bond distance between αR373-H_{m22} and ATP-$O_{\gamma 3}$ decreases by 0.29 Å, which causes the hydrogen bond between βR189-H_{m22} and ATP-$O_{\gamma 3}$ to loosen slightly leading to the strengthening of the interaction between βR189-H_{m12} and ATP-$O_{\gamma 2}$. Hence, β_{DP} exhibits a tight coordination of the equatorial phosphate oxygens by the two guanidinium groups of αR373 and βR189.

The Mulliken charges obtained in the transition state of β_{DP} (cf. Table 1) are similar to their counterparts in β_{TP} with the exception of Mg^{2+}, which transfers significantly less charge to its ligands as already noted in the case of the reactant state.

Intermediate state

After passing the transition state along the ATP hydrolysis reaction pathway, the system becomes trapped in an intermediate state conformation similarly to what is observed in the β_{TP} catalytic site. The intermediate state conformation is depicted in Fig. 3 *c* and reveals that this state is structurally characterized by bond formation between the nucleophilic oxygen and P_γ as well as completion of proton transfer from the hydronium ion toward the γ-phosphate group. The WAT1-O–P_γ distance decreases from 2.01 Å to 1.89 Å leading to complete bond formation, whereas the bond between ATP-$O_{\beta 3}$ and P_γ lengthens only slightly by 0.03 Å. Hence, neither the β_{TP} nor the β_{DP} binding pockets support rapid separation of ADP and P_i after the hydrolysis event has taken place but rather stabilize a near pentacovalent conformation of the phosphate backbone that would be energetically unfavorable in a solvent environment.

Final state

The structure of the final state is depicted in Fig. 3 *d* and corresponds to the lowest energy conformation we were able to obtain using the intermediate structure as starting point. Strikingly, this state, too, is characterized by a near pentacovalent arrangement of the γ-phosphate group without any significant separation along the P_γ–$O_{\beta 3}$ bond as observed in the case of β_{TP}. The tight confinement of the phosphate backbone by the binding pocket prevents further separation of products and rather stabilizes the observed conformation. Compared to the intermediate state, the $O_{\beta 3}$–P_γ bond is further elongated, but not completely broken, and has a length of 2.07 Å. The most notable structural difference compared to the intermediate state is a rearrangement in the hydrogen bonding network involving and surrounding P_i. The hydrogen on P_i derived from the nucleophilic water, WAT1, rotates around the P_γ–WAT1-O bond and hydrogen bonds to βE188. WAT3 and WAT2 reorganize their hydrogen bonds with each other and the nucleophilic oxygen: WAT2 replaces its hydrogen bond to the nucleophilic oxygen by a bond to WAT3-O, and the latter in turn changes its hydrogen bonding from WAT2 to the nucleophilic oxygen. This rearrangement pulls the side chain of βE188 toward P_γ by 0.32 Å and engages βE188 in a very tight coordination with P_i and its associated water molecules. As a result, the hydrogen bonding network surrounding P_i in the final state of β_{DP} differs considerably from the one in β_{TP}.

Energetics

The structural analysis presented above revealed that even though there are no larger scale conformational changes between β_{DP} and β_{TP}, both sites differ in important aspects in their local arrangement of binding pocket residues involved in catalysis and of associated water molecules. This is reflected in the respective energetics of ATP

hydrolysis in β_{TP} and β_{DP} as shown in Fig. 4. It can be seen that the transition state barrier in β_{DP} depicted in Fig. 4 *b* is reduced by 7 kcal/mol, namely from 25 kcal/mol in β_{TP} to a value of 18 kcal/mol. Using transition state theory, the barrier height in β_{DP} leads to hydrolysis rates in agreement with experimentally measured values.

The simulations show that in both β_{TP} and β_{DP} the nucleophilic attack of WAT1 via a multicenter proton-relay mechanism is energetically much preferable compared to direct proton transfer. Such a proton relay mechanism, therefore, appears to be a generic feature of the catalytic binding pockets in F_1 and is made possible by a preformed solvent environment present in the catalytic sites.

The intermediate state is energetically ~5 kcal/mol below the transition state and still in a high energy conformation. The reduction in energy is mainly due to bond formation between the nucleophilic oxygen and P_γ and proton transfer from the hydronium ion toward the phosphate oxygen.

Interestingly, the rearrangement of the hydrogen bonding network upon going from the intermediate to the final state leads to a major relaxation of the system and to an exothermic final state energy of −0.8 kcal/mol. Accordingly, the product and reactant states for ATP hydrolysis in β_{DP} are approximately equienergetic, which is in marked contrast to the situation in β_{TP} where ATP hydrolysis is found to be endothermic.

Finally, it should be mentioned that it was not possible to estimate the barriers between the reactant and the prehydrolysis state or between the intermediate and the final state. This would have required a multitude of constrained optimizations to model the movement and rotation of multiple water molecules and was computationally too demanding. The transitions between the respective conformations consist of the breaking and reformation of hydrogen bonds. Our previous study (Dittrich et al., 2003) has shown that upper limits for the corresponding barriers are in the range of 3–4 kcal/mol at the MP2//HF/6-31G level of theory. Furthermore, the comparison of the energetics in β_{TP} obtained via MP2//HF/6-31G and the B3LYP/6-31G level of theory showed that the relative magnitudes of the observed barriers are similar. One can, therefore, conclude that these barriers will not constitute rate limiting steps along the hydrolysis reaction pathway and can be left undetermined.

Interactions between QM and MM regions

Fig. 5 *b* shows the difference in Coulomb interaction between the prehydrolysis and the transition state between the QM core and the MM region. A comparison of these results with the ones for β_{TP} given in Fig. 5 *a* shows that the interaction pattern is similar and differs mainly in the appearance of an additional peak at position 109. The latter is due to the side chain of αR373 that in β_{DP} is coordinated toward the phosphate backbone. The sizeable magnitude of αR373's electrostatic transition state stabilization in β_{DP} provides evidence for its importance in promoting efficient ATP hydrolysis in β_{DP}. As in β_{TP}, the side chains of βK162 and βE188 stabilize the transition state due to a shift of negative charge from the γ- to the β-phosphate group in ATP and accumulation of positive charge on the hydronium ion, respectively. The side chain of βR260 provides some destabilization due to its net positive charge combined with its proximity to the hydronium ion.

It is important to notice that whereas the arginine finger residue βR373 contributes −21 kcal/mol of stabilization energy toward the transition state, its immediate neighbor, the guanidinium group of βR189, provides a mere −5.8 kcal/mol. Hence βR189 does not seem to be a major factor in transition state stabilization and rather ensures proper binding and orientation of the nucleotide inside the binding pocket.

Study of mutations αR373G and βR260C

Further characterization of the role of the positively charged residues αR373 and βR260 during ATP hydrolysis in β_{DP} was accomplished by examining the mutations αR373G and βR260C that have also been studied experimentally (Nadanaciva et al., 1999; Le et al., 2000; Parsonage et al., 1987). The reactant and final state structures of both mutants were fully reoptimized; as explained in Methods, the determination of the transition state structures was not possible, but in combination with the interaction energy

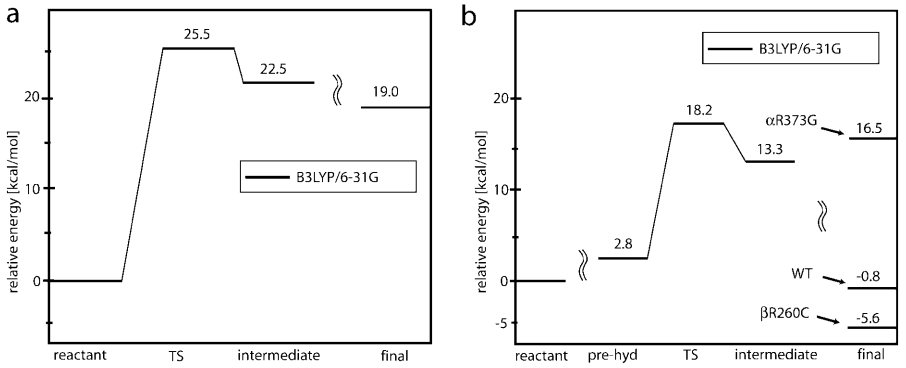

FIGURE 4 Energies along the reaction path. Shown are the energies along the ATP hydrolysis reaction coordinate in β_{TP} (*a*), and in β_{DP} (*b*). The reaction energetics in β_{DP} (*b*) include the final state energies for the wild-type system (*WT*) as well as for the mutants αR373G and βR260C. *TS* denotes the transition state and *pre-hyd* a pre-hydrolyzed state (see text).

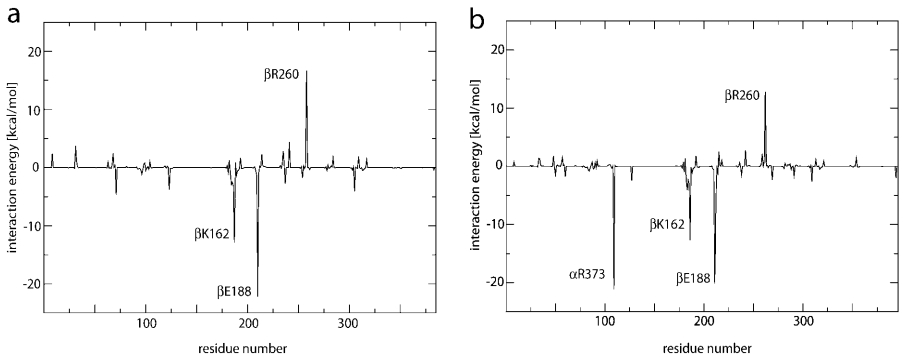

FIGURE 5 Electrostatic interaction between QM core and MM segment. Shown in *a* is the difference in Coulomb interaction between reactant and transition state in β_{TP}, and in *b* the difference between prehydrolysis state and transition state in β_{DP}. Since the QM/MM subsystem contains residues from α-, β-, and γ-subunits, the residue numbering scheme is different from the one in the original pdb structure.

analysis reported in Fig. 5, the reactant and final state energies provide an approximate picture of the residues' roles. Upon optimization, both mutated systems exhibited only minor changes in their conformation. The root mean-squared deviation for the QM segment between the wild-type and mutated systems are 0.09 Å and 0.19 Å for αR373G and βR260C, respectively. Fig. 4 shows the relative final state energies obtained for αR373G and βR260C. For αR373G, one observes a significant increase in the final state energy, thereby yielding an endothermic reaction profile. As discussed above, αR373 stabilizes the transition state electrostatically, and the mutation αR373G, therefore, can be expected to increase the transition state barrier giving rise to energetics very similar to what are observed in the β_{TP} pocket. The mutation βR260C exhibits a less dramatic effect on the reaction energetics and causes further lowering of the final state energy by ~5 kcal/mol. Since the positively charged guanidinium group of βR260 destabilizes the transition state (cf. Fig. 5), its replacement by the neutral cysteine can be expected to cause a reduction in barrier height. Hence, the mutation βR260C should give rise to both a more efficient catalytic reaction pathway and a more stable final state energy compared to the wild-type system.

DISCUSSION

This QM/MM study used an ab initio QM methodology (B3LYP/6-31G) to investigate the ATP hydrolysis reaction in the β_{TP} and β_{DP} catalytic sites of F_1-ATPase. The simulation results provide a description of the respective reaction pathways, their energetics, and the roles played by specific residues of the binding pockets for efficient hydrolysis and for conformational coupling to neighboring catalytic sites and the γ-stalk. The following sections will discuss the findings in the context of available structural and biochemical data and relate them to rotatory catalysis in F_1-ATPase.

ATP hydrolysis in the catalytic sites of F_1-ATPase

Several important aspects of rotatory catalysis in F_1-ATPase have not yet been rationalized in terms of available structural and biochemical data. Among them is the question how the catalytic binding pockets achieve efficient catalysis and are able to couple the chemical reaction to larger scale conformational changes eventually leading to rotation of the central stalk. In this context it also needs to be clarified how the three catalytic sites achieve cooperativity to engage in multisite catalysis with all three binding pockets occupied by nucleotide. Finally, the question if force generation during rotatory catalysis is due to the chemical reaction itself (Weber et al., 2000; Weber and Senior, 2003) or rather provided by ATP binding and/or ADP or P_i unbinding (Kinosita et al., 2000; Yasuda et al., 2001; Shimabukuro et al., 2003; Nishizaka et al., 2004) has yet to be answered conclusively, even though it seems that the latter view is favored.

Based on a pronounced endothermic reaction energy profile, our previous study of ATP hydrolysis in β_{TP} (Dittrich et al., 2003) supported the view that the chemical step itself is not energy linked. Furthermore, we proposed a novel multicenter proton relay mechanism as one means by which the catalytic sites achieve efficient catalysis. In this study, we examined both the β_{TP} and β_{DP} binding pocket of F_1-ATPase at a more advanced level of theory for the QM segment. This yielded insight into the catalytic properties of two distinct conformations along the rotatory catalytic cycle.

The β_{TP} pocket clearly exhibits features expected from a site binding ATP in a tight fashion. The overall reaction energy profile is strongly endothermic, thereby favoring the binding of ATP over products ADP and P_i. The barrier between the ATP reactant state and a hydrolyzed product state containing ADP and P_i is ~25 kcal/mol (cf. Fig. 4 *a*). Even though the chemical reaction itself does not constitute the rate-limiting step during ATP hydrolysis (Al-Shawi et al., 1989; Nakamoto et al., 2000), its transition state barrier constitutes a lower limit for the achievable rates. Using the well known rate expression derived from transition state theory (Fersht, 1999), the above energy barrier would give rise to a rate of $\sim 10^{-6}$ s^{-1}. It is therefore clear that β_{TP} is not able to sustain experimentally measured steady-state or even unisite turnover rates that are on the order of 10^2 s^{-1} and 10^{-4} s^{-1}, respectively (Al-Shawi et al., 1989, 1990).

Hence, the β_{TP} binding pocket examined in this study is not in a catalytically active conformation. It likely corresponds to the high affinity site proposed by Senior

et al. (2002) that evolves from the empty site upon binding of ATP followed by a rotation of the γ-stalk. ATP hydrolysis will then take place upon further conformational changes of β_{TP} toward β_{DP} induced by ATP binding to the empty site and, likely, further rotation of the γ-stalk.

Such a scenario is supported by our study of the β_{DP} binding pocket that captures the catalytic site at a later stage along the rotatory catalytic cycle. As shown in Fig. 4, the energetics of ATP hydrolysis change from being strongly endothermic in β_{TP} to being approximately equienergetic in β_{DP} together with a significant decrease in the energy of the transition state. Using the barrier height of 18.2 kcal/mol between the reactant and the transition state combined with the rate constant expression of transition state theory (Fersht, 1999), one obtains a reaction rate of $k \sim 1\ s^{-1}$. This corresponds to an increase by six orders of magnitude compared to β_{TP}. A rate of $k \sim 1\ s^{-1}$ in β_{DP} is in accord with unisite measurements on beef heart mitochondria by Grubmeyer et al. (1982) but is slightly too low to accommodate the observed multisite turnover rates in either the mitochondrial or the *Escherichia coli* enzymes. Since, energetically, the difference between the calculated and measured rates corresponds to only a few kilocalories per mol, they are beyond our computational accuracy and may be accounted for by, e.g., entropic contributions and zero point corrections missing from our description.

Overall, the simulations clearly show that the β_{DP} catalytic sites captured in the crystallographic structure of Gibbons et al. (2000) are in a state competent for hydrolysis of ATP. It is remarkable that conformational changes between β_{TP} and β_{DP} can lead to such drastic changes in the overall energetics. This is further highlighted by the fact that the structural changes between both conformations are, with the exception of the large movement of the side chain of αR373, only minor and consist mostly of small structural rearrangements as discussed in Results. This stresses the importance of αR373's guanidinium group for catalysis and will be discussed in more detail in the next section.

The product state of ATP hydrolysis in β_{DP} is shown in Fig. 3 *d* and reveals that ADP and P_i do not separate appreciably after the catalytic event has taken place, as would be expected in a solution environment due to their repelling charge. Rather, the tight confinement by residues of the binding pocket, e.g., βE188, βR189, βR260, and αS344 (cf. Fig. 2), keeps them close to each other and also maintains their mutual orientation. Hence, our simulations suggest that the binding pockets of F_1-ATPase, rather than providing a relatively open cavity in which product formation takes place in a combustive manner, are tightly coupled to the substrate over the whole course of the reaction and, thereby, exercise maximal control during each stage of the chemical transformation. Such a mechanism obviously has several advantages: It provides the enzyme with an exquisite probe of the instantaneous state along the reaction path in each binding pocket and, thereby, assists communication between catalytic sites during multisite catalysis. Furthermore, in the synthesis direction, the formation of ATP is greatly facilitated since the substrates ADP and P_i do not have to position themselves for bond formation but are already primed for reaction once the empty binding pocket closes upon substrate binding and changes its conformation toward β_{DP}.

The fact that our simulations yield an equienergetic reaction profile for ATP hydrolysis in β_{DP} supports the experimental finding that the chemical reaction itself is not energy linked and rather has an equilibrium constant of $K \sim 1$ (Grubmeyer et al., 1982; Cross et al., 1982). Experimentally, this is strictly known only under unisite conditions. Assuming that the crystal structure underlying our simulations represents a snapshot taken during multisite catalysis, our simulations suggest that a conformation giving rise to an equilibrium constant of $K \sim 1$ for the chemical step also appears in β_{DP} during steady-state catalysis. In agreement with our results, Strajbl et al. (2003) have recently examined the ATP hydrolysis reaction in F_1-ATPase using an EVB method and found that β_{DP} exhibits an approximately equienergetic reaction energy profile.

Recent high resolution single molecule studies (Yasuda et al., 2001; Shimabukuro et al., 2003; Nishizaka et al., 2004) have revealed that a 120° rotation of the γ-stalk, which consumes one ATP molecule, consists of 90° and 30° substeps, which were later revised to 80° and 40°. In these studies, the authors used catalytic site mutations and variations in ATP concentration to identify two distinct dwell intervals. The first dwell precedes the 90° (80°) substep and was attributed to ATP binding. The interim dwell takes place before the second substep and includes the hydrolysis reaction (Shimabukuro et al., 2003). Since the x-ray crystallographic structure that was used as the starting model of our study was not inhibited using transition state analogs, it likely has a conformation close to the first dwell. Accordingly, the β_{DP} conformation investigated by us may not directly correspond to that of the interim dwell where the actual hydrolysis takes place but rather be considered as the one after the 30° (40°) substep. The overall scenario is summarized in Table 2.

Nevertheless, the efficient hydrolysis reaction profile revealed in this study suggests that the structure of the binding pocket in β_{DP} closely resembles that of the interim dwell conformation. One may therefore conclude that during the 30° (40°) substep this subunit does not undergo conformational changes that significantly alter the reaction energy profile, such as the movement of the arginine finger αR373. Hence, it follows that such conformational changes take place during the first 90° (80°) substep. Single molecule experiments have also suggested that the 30° (40°) substep is likely coupled to the release of the product P_i from the binding pocket (Yasuda et al., 2001; Shimabukuro et al., 2003; Nishizaka et al., 2004). Thus, during hydrolysis, the product state has to provide free energy to allow for a spontaneous release of P_i. Unfortunately, the P_i release process cannot be

TABLE 2 Events during rotatory catalysis

Event	Binding dwell	90° rotation	Intermediate dwell	30° rotation
Interpretation	ATP waiting state; corresponds to our structure	Closing of empty site upon ATP binding	ATP hydrolysis	Product unbinding

Listed are the steps observed by Shimabukuro et al. (2003) during a single 120° rotation and their interpretation. After completion of the 30° rotation, the system starts over in the binding dwell.

directly simulated by our method. It should be noted, however, that the equienergetic reaction profile revealed by this study, as opposed to a strongly exothermic one, has several advantages for P_i release: assuming a negligible change in entropy between reactant and product state, the equienergetic profile ensures that the cleavage of ATP can take place in the binding pocket, and, at the same time, allows the product state to retain maximal free energy for the subsequent step, i.e., P_i release.

It has been pointed out (Senior et al., 2002) that an equilibrium constant of $K \sim 1$ causes equal amounts of reactant (ATP) and product (ADP/P_i) to be present in the binding pocket, thereby giving rise to inefficient hydrolysis. Hence, to increase the overall catalytic efficiency, a mechanism that enforces release of the product species has to be involved. The study by Shimabukuro et al. (2003) has shown that ATP hydrolysis takes place during the interim dwell and, therefore, without inducing large conformational rearrangements. Only minor structural changes of the catalytic sites are therefore involved in signaling the presence of the correct product state. Tight coordination of the substrate by the binding pocket enhances the sensitivity to such small motions, and we thus suggest that the close proximity of catalytic site residues allows the enzyme to ensure that its rotatory catalytic cycle continues only if product is present and can subsequently be released. Incidentally, the binding pocket does not promote true formation of ADP and P_i but rather stabilizes a closely coordinated final state. This greatly facilitates the coupling of the enzyme to the substrate and, likely, is important for the reversibility of the catalytic reaction in F_1-ATPase.

Similarly to our previous study, our new simulations show that the hydrolysis pathways proceeding via a multicenter proton relay mechanism are energetically more favorable (by ~13 kcal/mol in β_{DP}) than direct proton transfer from the nucleophilic water toward ATP. A similar ''two-water model'' has been proposed by Scheidig et al. (1999) for $p21^{ras}$ based on x-ray crystal structures. A recent QM/MM study of ATP hydrolysis in myosin also suggests an efficient multicenter proton relay through a nearby hydroxy group of a serine residue (Li and Cui, 2004). This suggests that an essential ingredient of the catalytic sites in F_1 and other molecular motors to achieve efficient catalysis is the provision of an environment facilitating such a multicenter proton pathway.

In contrast to these results, Strajbl et al. (2003) find that in the framework of EVB nucleophilic attack of a single water molecule is sufficient to obtain reaction barriers in agreement with experiment. Although the EVB treatment models true free energy surfaces and, therefore, may be superior to the enthalpic calculations of this study, the authors did not consider the possibility of a multicenter proton relay mechanism using their EVB method. Hence no conclusive statement about the energetically most favorable mechanism can be drawn from their study.

As seen in Fig. 5 and also shown previously (Dittrich et al., 2003), the transition state of the multicenter reaction path involves a hydronium ion strongly stabilized by a negatively charged glutamate, βE188. Thus, βE188 plays a crucial role in facilitating ATP hydrolysis via the multicenter proton relay mechanism. This agrees well with a mutation study by Amano et al. (1994) that revealed that replacements of βE190 in F_1 from a thermophilic organism (corresponding to βE188 in MF_1) by either a glutamine or an aspartate impairs and significantly slows down the hydrolysis reaction, respectively. Hence, the close coordination of the negatively charged carboxylate of βE188 to the hydronium ion in the transition state revealed in our study is essential for efficient catalysis.

Role of specific binding pocket residues during rotatory catalysis

Quantum mechanically derived RESP charges for a reduced QM system were used to obtain a classical approximation of the Coulomb interactions between the catalytic core region and the protein environment (cf. Methods and Fig. 5). Both β_{TP} and β_{DP} exhibit a very similar interaction pattern, the major difference deriving from the proximity of αR373's guanidinium group to ATP's phosphate backbone in β_{DP}. Fig. 5 clearly shows that in β_{DP} αR373 furnishes a key residue for transition state stabilization and, thereby, contributes to the decrease in transition state barrier height with respect to β_{TP}. This likely is of significance for the overall mechanism of F_1-ATPase.

To examine αR373's role during catalysis in β_{DP} further, we simulated the mutation αR373G. The removal of the guanidinium group of αR373 from the phosphate backbone leads to a drastic increase in final state energy (cf. Fig. 4), shifting the overall reaction equilibrium from slightly exothermic to strongly endothermic, similar to the energetics observed in β_{TP}. The reaction energy profile in β_{TP} can, therefore, to a large degree be attributed to the absence of αR373's guanidinium group. Hence, our simulations clearly

highlight two essential functions of αR373 for rotatory catalysis. First, and in agreement with experimental findings (Nadanaciva et al., 1999), our study of the electrostatic interactions shows that the proximity of the residue's guanidinium group to the phosphate backbone is essential for stabilization of the transition state to achieve physiological rates of ATP hydrolysis. Second, the strong impact of αR373 on the reaction equilibrium as revealed by our mutation study suggests a role in the communication between neighboring catalytic sites as proposed by Nadanaciva et al. (1999) and Le et al. (2000). Since thermodynamically the chemical reaction will not proceed in the presence of an endothermic final state energy, the distance of αR373's side chain to the phosphate backbone provides the enzyme with an exquisite control mechanism to synchronize its three catalytic binding pockets during steady-state rotatory catalysis.

In light of the dramatic change of the reaction energy profile and the overall structural similarity of the mutant αR373G catalytic site to the wild-type system (root mean-square deviation (RMSD) 0.09 Å; cf. Results), one can conjecture that the most significant contribution of αR373's guanidinium group to the catalytic reaction is mostly electrostatic in nature. This suggests that ATP hydrolysis inside the binding pockets of F_1 is largely controlled via electrostatic interactions by the protein environment. The importance of electrostatic effects for catalysis in enzymes has been advocated by Strajbl et al. (2003) and Yang et al. (2003) and found to be important for ATP hydrolysis in F_1.

Interestingly, Le et al. (2000) have shown that under unisite conditions αR373 does not participate in the catalytic reaction. In light of our findings, this suggests that the β_{DP} binding site studied by us is in a conformation different from the one present experimentally under unisite conditions. It is, e.g., conceivable that experimentally residues other than αR373 can at least partially compensate for its loss, making it difficult to assign unique roles for ATP hydrolysis to specific residues via mutation studies.

The second mutation analyzed in the β_{DP} catalytic site was βR260C. Several experimental studies have investigated the effect of mutating βR260 on rotatory catalysis in F_1-ATPase. Noumi et al. (1986) showed that the mutation βR260H greatly reduces the promotion of multisite catalysis and also leads to an increase in the rate of release of P_i. Additional studies (Parsonage et al., 1987; Al-Shawi et al., 1990) revealed that the mutation βR260C suppresses multisite catalysis even more than does βR260H. Furthermore, investigation of the kinetics of several β-subunit mutations in *E. coli* (Al-Shawi et al., 1990) uncovered that the catalytic rates k_2 and k_{-2} in βR260C are reduced by a factor of $\sim$30 and $\sim$2, respectively, yielding an equilibrium constant K_2 of 0.073. This value corresponds to a free energy difference between reactant and product of $\sim$2 kcal/mol; the change in the transition state barrier is of the same magnitude.

The calculated changes in electrostatics between the reactant and transition state for the βR260C mutation shown in Fig. 5 paint a different picture. Even though the values given provide only estimates for the true interaction energies, they clearly reveal a significant destabilization of the transition state by βR260. This destabilization, to a large degree, is due to the positive charge on the hydronium ion present in the transition state; the mutation βR260C, therefore, is predicted to cause a rate increase rather than the experimentally observed reduction. It is possible, however, that the experimental removal of the guanidinium group leads to a destabilization of the catalytic glutamate βE188, thereby compensating for a decrease in Coulomb repulsion due to βR260. Such a destabilization might be caused by larger scale rearrangements inside the binding pocket caused by the removal of the bulky guanidinium group and that are, due to their magnitude, not captured in our simulations.

Furthermore, the simulations of βR260C in β_{DP} show that removal of the arginine leads to a slight stabilization of the final state (cf. Fig. 4) in contrast to the experimentally observed decrease in K_2. As argued above, this indicates that due to structural rearrangements caused by the mutations the experimentally probed conformation might be different from the one investigated in this study.

Unfortunately, it is not straightforward to interpret the simulation result for βR260C in terms of the mutation's disruptive effect on multisite catalysis. In light of the reduction in final state energy it is conceivable, however, that a necessary requirement for multisite catalysis is an equienergetic reaction profile, distortion of which will cause a breakdown of this mode of operation.

CONCLUSIONS

In this publication, we report the findings of QM/MM simulations of ATP hydrolysis in the β_{TP} and β_{DP} catalytic sites of F_1-ATPase. Either site captures the binding pocket at a different stage along the rotatory catalytic cycle, β_{DP} being farther along in the process. Consistent with this fact, we find that whereas β_{TP} does not foster ATP hydrolysis and strongly favors the presence of ATP over ADP and P_i, the β_{DP} site does promote ATP hydrolysis at experimental rates with an equilibrium constant of $K \sim 1$. Efficient hydrolysis in the catalytic sites is found to proceed via a multisite proton relay mechanism as previously suggested by us. Rather unexpectedly, we find that over the whole course of the chemical reaction the substrate is tightly coordinated by protein residues, and the products ADP and P_i do not separate appreciably after hydrolysis has taken place. We suggest that this constitutes a control mechanism by which, e.g., the enzyme ensures that only products ADP and P_i and not ATP are released during the near equilibrium reaction. The tight coordination might also be responsible for F_1's ability to reversibly hydrolyze and synthesize ATP.

The investigation of the electrostatic interactions between the catalytic core region and the protein environment showed that αR373 plays an important role for transition state

stabilization. Simulations of the mutation αR373G revealed that αR373 also considerably influences the reaction equilibrium, which suggest an additional role for communication between catalytic sites. In light of experimental mutation studies, our simulations for αR373G and βR260C suggest that the investigated structures are different from the ones probed experimentally, which likely undergo larger scale conformational changes caused by the mutations.

The authors thank Dr. Tajkhorshid for providing the equilibrated F_1 structure and Mr. Kaneko for the QM/MM implementation into GAMESS. The molecular images in this article were created with the molecular graphics program VMD (Humphrey et al., 1996). The preparation of this publication was greatly facilitated by BioCoRE (Bhandarkar et al., 1999). We thank Ralph Roskies and the Pittsburgh Supercomputer Center for continuous support and acknowledge the use of the Center's GS1280 computational facilities made available by the National Center for Research Resources (NCRR) Research Resource RR06009.

This work was supported by the National Institutes of Health (grant PHS 5 P41 RR05969), the National Science Foundation (grant 0234938), and the Japan Science and Technology Agency. The authors also acknowledge computer time provided by the National Resource Allocations Committee (grant MCA93S028).

REFERENCES

Abrahams, J., A. Leslie, R. Lutter, and J. Walker. 1994. Structure at 2.8 Å resolution of F_1-ATPase from bovine heart mitochondria. *Nature.* 370:621–628.

Aksimentiev, A., I. A. Balabin, R. H. Fillingame, and K. Schulten. 2004. Insights into the molecular mechanism of rotation in the F_o sector of ATP synthase. *Biophys. J.* 86:1332–1344.

Al-Shawi, M. K., D. Parsonage, and A. E. Senior. 1989. Kinetic characterization of the unisite catalytic pathway of seven β-subunit mutant F_1-ATPases from *Escherichia coli*. *J. Biol. Chem.* 264:15376–15383.

Al-Shawi, M. K., D. Parsonage, and A. E. Senior. 1990. Thermodynamic analyses of the catalytic pathway of F_1-ATPase from *Escherichia coli*. *J. Biol. Chem.* 265:4402–4410.

Amano, T., K. Tozawa, M. Yoshida, and H. Murakami. 1994. Spatial precision of a catalytic carboxylate of F_1-ATPase β subunit probed by introducing different carboxylate-containing side chains. *FEBS Lett.* 348:93–98.

Angevine, C. M., and R. H. Fillingame. 2003. Aqueous access channels in subunit *a* of rotary ATP synthase. *J. Biol. Chem.* 278:6066–6074.

Baily, C., P. Cieplak, W. Cornell, and P. Kollman. 1993. A well-behaved electrostatic potential-based method using charge restraints for deriving atomic charges: the RESP model. *J. Phys. Chem.* 97:10269–10280.

Bernal-Uruchurtu, M. I., and I. Ortega-Blake. 1995. A refined Monte Carlo study of Mg^{2+} and Ca^{2+} hydration. *J. Chem. Phys.* 103:1588–1598.

Bhandarkar, M., G. Budescu, W. Humphrey, J. A. Izaguirre, S. Izrailev, L. V. Kalé, D. Kosztin, F. Molnar, J. C. Phillips, and K. Schulten. 1999. BioCoRE: a collaboratory for structural biology. *In* Proceedings of the SCS International Conference on Web-Based Modeling and Simulation. A. G. Bruzzone, A. Uchrmacher, and E. H. Page, editors. San Francisco, CA. 242–251.

Böckmann, R. A., and H. Grubmüller. 2002. Nanoseconds molecular dynamics simulation of primary mechanical energy transfer steps in F_1-ATP synthase. *Nat. Struct. Biol.* 9:198–202.

Boyer, P. D. 1993. The binding change mechanism for ATP synthase–some probabilities and possibilities. *Biochim. Biophys. Acta.* 1140:215–250.

Boyer, P. D. 1997. The ATP synthase—a splendid molecular machine. *Annu. Rev. Biochem.* 66:717–749.

Cavalli, A., and P. Carloni. 2002. Enzymatic GTP hydrolysis: insights from an ab initio molecular dynamics study. *J. Am. Chem. Soc.* 124:3763–3768.

Cornell, W. D., P. Cieplak, C. I. Bayly, I. R. Gould, J. K. M. Merz, D. M. Ferguson, D. C. Spellmeyer, T. Fox, J. W. Caldwell, and P. A. Kollman. 1995. A second generation force field for the simulation of proteins, nucleic acids, and organic molecules. *J. Am. Chem. Soc.* 117:5179–5197.

Cross, R. L. 2000. The rotary binding change mechanism of ATP synthases. *Biochim. Biophys. Acta.* 1458:270–275.

Cross, R. L., C. Grubmeyer, and H. S. Penefsky. 1982. Mechanism of ATP hydrolysis by beef heart mitochondrial ATPase. Rate enhancements resulting from cooperative interactions between multiple catalytic sites. *J. Biol. Chem.* 257:12101–12105.

Dittrich, M., S. Hayashi, and K. Schulten. 2003. On the mechanism of ATP hydrolysis in F_1-ATPase. *Biophys. J.* 85:2253–2266.

Fersht, A. 1999. Structure and Mechanism in Protein Science. W. H. Freeman and Co., New York.

Field, M. J., P. A. Bash, and M. Karplus. 1990. A combined quantum mechanical and molecular mechanical potential for molecular dynamics simulations. *J. Comp. Chem.* 11:700–733.

Fillingame, R. H., C. M. Angevine, and O. Y. Dmitriev. 2002. Coupling proton movements to *c*-ring rotation in F_1F_o ATP synthase: aqueous access channels and helix rotations at the *a-c* interface. *Biochim. Biophys. Acta.* 1555:29–36.

Gao, Y. Q., W. Yang, R. A. Marcus, and M. Karplus. 2003. A model for the cooperative free energy transduction and kinetics of ATP hydrolysis by F_1-ATPase. *Proc. Natl. Acad. Sci. USA.* 100:11339–11344.

Gibbons, C., M. G. Montgomery, A. G. W. Leslie, and J. E. Walker. 2000. The structure of the central stalk in bovine F_1-ATPase at 2.4 *Å* resolution. *Nat. Struct. Biol.* 7:1055–1061.

Glennon, T. M., J. Villà, and A. Warshel. 2000. How does GAP catalyze the GTPase reaction of Ras?: a computer simulation study. *Biochemistry.* 39:9641–9651.

Grubmeyer, C., R. L. Cross, and H. S. Penefski. 1982. Mechanism of ATP hydrolysis by beef heart mitochondrial ATPase. Rate constants for elementary steps in catalysis at a single site. *J. Biol. Chem.* 257:12092–12100.

Hayashi, S., E. Tajkhorshid, E. Pebay-Peyroula, A. Royant, E. M. Landau, J. Navarro, and K. Schulten. 2001. Structural determinants of spectral tuning in retinal proteins – bacteriorhodopsin vs sensory rhodopsin II. *J. Phys. Chem. B.* 105:10124–10131.

Humphrey, W., A. Dalke, and K. Schulten. 1996. VMD—visual molecular dynamics. *J. Mol. Graph.* 14:33–38.

Junge, W., H. Lill, and S. Engelbrecht. 1997. ATP synthase: an electrochemical transducer with rotatory mechanics. *Trends Biochem. Sci.* 22:420–423.

Kinosita, K., Jr., R. Yasuda, and K. Adachi. 2000. A rotary molecular motor that can work at near 100% efficiency. *Philos. Trans. R. Soc. Lond. B.* 355:473–489.

Langen, R., T. Schweins, and A. Warshel. 1992. On the mechanism of guanosine triphosphate hydrolysis in *ras* p21 proteins. *Biochemistry.* 31:8691–8696.

Le, N. P., H. Omote, Y. Wada, M. K. Al-Shawi, R. K. Nakamoto, and M. Futai. 2000. *Escherichia coli* ATP synthase α subunit Arg-376: the catalytic site arginine does not participate in the hydrolysis/synthesis reaction but is required for promotion to the steady state. *Biochemistry.* 39:2778–2783.

Li, G., and Q. Cui. 2004. Mechanochemical coupling in myosin: A theoretical analysis with molecular dynamics and combined QM/MM reaction path calculations. *J. Phys. Chem. B.* 108: 3342–3357.

Lyne, P. D., M. Hodoscek, and M. Karplus. 1999. A hybrid QM-MM potential employing Hartree-Fock or density functional methods in the quantum region. *J. Phys. Chem. A.* 103:3462–3471.

Menz, R. I., J. E. Walker, and A. G. W. Leslie. 2001. Structure of bovine mitochondrial F_1-ATPase with nucleotide bound to all three catalytic

sites: implications for the mechanism of rotary catalysis. *Cell.* 106:331–341.

Minehard, T. J., N. Marzari, R. Cooke, E. Pate, P. A. Kollman, and R. Car. 2002. A classical and ab initio study of the interaction of the myosin triphosphate binding domain with ATP. *Biophys. J.* 82:660–675.

Nadanaciva, S., J. Weber, S. Wilke-Mounts, and A. E. Senior. 1999. Importance of F_1-ATPase residue α-Arg-373 for catalytic transition state stabilization. *Biochemistry.* 38:15493–15499.

Nakamoto, R. K., C. J. Ketchum, P. H. Kuo, Y. B. Peskova, and M. K. Al-Shawi. 2000. Molecular mechanisms of rotational catalysis in the F_oF_1 ATP synthase. *Biochim. Biophys. Acta.* 1458:289–299.

Nishizaka, T., K. Oiwa, H. Noji, S. Kimura, E. Muneyuki, M. Yoshida, and K. Kinosita, Jr. 2004. Chemomechanical coupling in F_1-ATPase revealed by simultaneous observation of nucleotide kinetics and rotation. *Nat. Struct. Mol. Biol.* 11:142–148.

Noji, H., T. Yasuda, M. Yoshida, and K. Kinosita, Jr. 1997. Direct observation of the rotation of F_1-ATPase. *Nature.* 386:299–302.

Noumi, T., M. Taniai, H. Kanazawa, and M. Futai. 1986. Replacement of arginine 246 by histidine in the β subunit of *Escherichia coli* H^+-ATPase resulted in loss of multi-site ATPase activity. *J. Biol. Chem.* 261:9196–9201.

Okimoto, N., K. Yamanaka, J. Ueno, M. Hata, T. Hoshino, and M. Tsuda. 2001. Theoretical studies of the ATP hydrolysis mechanism of myosin. *Biophys. J.* 81:2786–2794.

Parsonage, D., T. M. Duncan, S. Wilke-Mounts, F. A. S. Kironde, L. Hatch, and A. E. Senior. 1987. The defective proton-ATPase of *uncD* mutants of *Escherichia coli*. *J. Biol. Chem.* 262:6301–6307.

Rastogi, V. K., and M. E. Girvin. 1999. Structural changes linked to proton translocation by subunit *c* of the ATP synthase. *Nature.* 402:263–268.

Ren, H., and W. S. Allison. 2000. On what makes the γ subunit spin during ATP hydrolysis by F_1. *Biochim. Biophys. Acta.* 1458:221–233.

Scheidig, A. J., C. Burmester, and R. S. Goody. 1999. The pre-hydrolysis state of $p21^{ras}$ in complex with GTP: new insights into the role of water molecules in the GTP hydrolysis reaction of ras-like proteins. *Structure.* 7:1311–1324.

Schmidt, M. W., K. K. Baldridge, J. A. Boatz, S. T. Elbert, M. S. Gordon, J. H. Jensen, S. Koseki, N. Matsunaga, K. A. Nguyen, S. Su, T. L. Windus, M. Dupuis, and J. J. A. Montgomery. 1993. The general atomic and molecular electronic structure system. *J. Comp. Chem.* 14:1347–1363.

Schweins, T., R. Langen, and A. Warshel. 1994. Why have mutagenesis studies not located the general base in *ras* p21 proteins? *Nat. Struct. Biol.* 1:476–484.

Senior, A. E., S. Nadanaciva, and J. Weber. 2002. The molecular mechanism of ATP synthesis by F_1F_o-ATP synthase. *Biochim. Biophys. Acta.* 1553:188–211.

Shimabukuro, K., R. Yasuda, E. Muneyuki, K. Y. Hara, K. Kinosita, Jr., and M. Yoshida. 2003. Catalysis and rotation of F_1 motor: cleavage of ATP at the catalytic site occurs in 1 ms before 40° substep rotation. *Proc. Natl. Acad. Sci. USA.* 100:14731–14736.

Singh, U. C., and P. A. Kollman. 1986. A combined *ab initio* quantum mechanical and molecular mechanical method for carrying out simulations on complex molecular systems: applications to the $CH_3Cl + Cl^-$ exchange reaction and gas phase protonation. *J. Comp. Chem.* 7:718–730.

Strajbl, M., A. Shurki, and A. Warshel. 2003. Converting conformational changes to electrostatic energy in molecular motors: the energetics of ATP synthase. *Proc. Natl. Acad. Sci. USA.* 100:14834–14839.

Warshel, A. 1976. Bicycle-pedal model for the first step in the vision process. *Nature.* 260:679–683.

Warshel, A. 1991. Computer Modeling of Chemical Reactions in Enzymes and Solutions. John Wiley and Sons, Inc., New York.

Warshel, A. 2003. Computer simulations of enzyme catalysis: methods, progress, and in sights. *Annu. Rev. Biophys. Biomol. Struct.* 32:425–443.

Weber, J., S. Nadanaciva, and A. E. Senior. 2000. ATP-driven rotation of the γ subunit in F_1-ATPase. *FEBS Lett.* 483:1–5.

Weber, J., and A. E. Senior. 2003. ATP synthesis driven by proton transport in F_1F_o-ATP synthase. *FEBS Lett.* 545:61–70.

Weber, J., S. Wilke-Mounts, and A. E. Senior. 1994. Cooperativity and stoichiometry of substrate binding to the catalytic sites of *Escherichia coli* F_1-ATPase. *J. Biol. Chem.* 269:20462–20467.

Wittinghofer, A., K. Scheffzek, and M. R. Ahmadian. 1997. The interaction of Ras with GTPase-activating proteins. *FEBS Lett.* 410:63–67.

Yang, W., Y. Gao, Q. Cui, J. Ma, and M. Karplus. 2003. The missing link between thermodynamics and structure in F_1-ATPase. *Proc. Natl. Acad. Sci. USA.* 100:874–879.

Yasuda, R., H. Noji, M. Yoshida, K. Kinosita, Jr., and H. Itoh. 2001. Resolution of distinct rotational substeps by submillisecond kinetic analysis of F_1-ATPase. *Nature.* 410:898–904.

Zhang, L., and J. Hermans. 1996. Hydrophilicity of cavities in proteins. *Proteins.* 24:433–438.